Release and Elementary Mechanisms of Nitric Oxide in Hair Cells

Ping Lv, Adrian Rodriguez-Contreras, Hyo Jeong Kim, Jun Zhu, Dongguang Wei, Sihn Choong-Ryoul, Emily Eastwood, Karen Mu, Snezana Levic, Haitao Song, Petrov Y. Yevgeniy, Peter J. S. Smith and Ebenezer N. Yamoah

J Neurophysiol 103:2494-2505, 2010. First published 10 March 2010; doi:10.1152/jn.00017.2010

J Neurophysiol 103: 2494–2505, 2010.
First published March 10, 2010; doi:10.1152/jn.00017.2010.

Release and Elementary Mechanisms of Nitric Oxide in Hair Cells

Ping Lv,[1,*] Adrian Rodriguez-Contreras,[1,*] Hyo Jeong Kim,[1] Jun Zhu,[2] Dongguang Wei,[1] Sihn Choong-Ryoul,[1] Emily Eastwood,[1] Karen Mu,[1] Snezana Levic,[1] Haitao Song,[1] Petrov Y. Yevgeniy,[1] Peter J. S. Smith,[3] and Ebenezer N. Yamoah[1,3]

[1]*Center for Neuroscience, Department of Anesthesiology and Pain Medicine, Program in Communication Science, University of California, Davis, Davis, California;* [2]*Department of Nephrology, Xijing Hospital, Fourth Military Medical University, Xi'an, China; and* [3]*BioCurrent Research Center, Marine Biological Laboratory, Woods Hole, Massachusetts*

Submitted 11 January 2010; accepted in final form 6 March 2010

Lv P, Rodriguez-Contreras A, Kim HJ, Zhu J, Wei D, Choong-Ryoul S, Eastwood E, Mu K, Levic S, Song H, Yevgeniy PY, Smith PJS, Yamoah EN. Release and elementary mechanisms of nitric oxide in hair cells. *J Neurophysiol* 103: 2494–2505, 2010. First published March 10, 2010; doi:10.1152/jn.00017.2010. The enzyme nitric oxide (NO) synthase, that produces the signaling molecule NO, has been identified in several cell types in the inner ear. However, it is unclear whether a measurable quantity of NO is released in the inner ear to confer specific functions. Indeed, the functional significance of NO and the elementary cellular mechanism thereof are most uncertain. Here, we demonstrate that the sensory epithelia of the frog saccule release NO and explore its release mechanisms by using self-referencing NO-selective electrodes. Additionally, we investigated the functional effects of NO on electrical properties of hair cells and determined their underlying cellular mechanism. We show detectable amounts of NO are released by hair cells (>50 nM). Furthermore, a hair-cell efferent modulator acetylcholine produces at least a threefold increase in NO release. NO not only attenuated the baseline membrane oscillations but it also increased the magnitude of current required to generate the characteristic membrane potential oscillations. This resulted in a rightward shift in the frequency–current relationship and altered the excitability of hair cells. Our data suggest that these effects ensue because NO reduces whole cell Ca^{2+} current and drastically decreases the open probability of single-channel events of the L-type and non L-type Ca^{2+} channels in hair cells, an effect that is mediated through direct nitrosylation of the channel and activation of protein kinase G. Finally, NO increases the magnitude of Ca^{2+}-activated K^+ currents via direct NO nitrosylation. We conclude that NO-mediated inhibition serves as a component of efferent nerve modulation of hair cells.

INTRODUCTION

Hair cells of vestibular and auditory systems are neuroepithelia cells and, like neurons, their electrical outputs are governed by intrinsic membrane properties and extrinsic synaptic inputs. However, unlike other primary sensory systems in which the stimulus is processed through a cascade of biochemical reactions, stimulation of hair cells is coupled directly to mechanical stimuli, making them decidedly prone to mechanical damage (Hudspeth and Logothetis 2000; Yoshida et al. 2000). To maintain its acute sensitivity and to protect itself against overstimulation (e.g., noise, vibration), the electrical gain of a hair cell is tweaked tightly through modulation of K^+ and Ca^{2+} conductances as well as efferent synaptic inhibitory feedback from the brain stem through activation of $\alpha9\alpha10$ nicotinic acetylcholine (ACh) receptors and a small conductance Ca^{2+}-activated K^+ current (Chen and Eatock 2000; Elgoyhen et al. 2001; Katz et al. 2004; Yoshida et al. 2000; Yuhas and Fuchs 1999). Whereas release of ACh at the efferent nerve terminals elicits a fast membrane hyperpolarization (Housley et al. 2006), prolonged stimulation of efferent nerves produces further delayed inhibition, whose mechanism remains elusive (Sridhar et al. 1997).

Nitric oxide (NO) is a diffusible second messenger, expressed in the nervous and cardiovascular systems, and regulates neurotransmission, serving as the principal endothelium-derived relaxing factor (Bredt et al. 1990; Stamler and Loscalzo 1992). The enzyme that forms NO from arginine, nitric oxide synthase (NOS), has been identified in the inner ear, although its physiological role remains unclear. The spiral modiolar artery may be one of the major sources of endogenous production of NO (Jiang et al. 2004). However, NOS is expressed not only in hair cells but also in afferent and efferent nerve terminals in a variety of animal models ranging from amphibians to mammals (Fessenden et al. 1994; Flores et al. 2001; Hess et al. 1998; Lysakowski and Singer 2000), raising the possibility that evolutionary preservation of the NO pathway is of vital importance to inner ear functions. Indeed, measurable amounts of NO release from the organ of Corti have been reported and the level is increased after noise exposure. Moreover, it is unknown whether the increase in NO levels following noise exposure serves a protective or pathological role (Shi et al. 2002). Nonetheless, the physiological significance of NO in hair cells may be derived from the effects of the reactive molecular messenger on their ionic conductances, although the net action of NO on ionic currents in hair cells is complex. On one hand, it has been demonstrated that NO inhibits a large conductance outward rectifier K^+ current ($I_{K,L}$) in type I hair cells in rat crista ampullaris (Chen and Eatock 2000), suggesting that NO produces an increase in membrane excitability. In contrast, NO reduces the magnitude of Ca^{2+} currents (Almanza et al. 2007), yielding an opposite effect on the membrane potential.

To further understand the sources and effects of NO on hair cells, we determined whether the frog saccule releases NO and identified its elementary mechanisms of actions. Here, we show that NO is released by the sensory epithelia and by ACh. On release NO regulates Ca^{2+} and K^+ channels in hair cells. Additionally, we provide evidence to demonstrate that NO modulates Ca^{2+} and K^+ channels by direct nitrosylation.

* These authors contributed equally to this work.

Address for reprint requests and other correspondence: E. N. Yamoah, Center for Neuroscience, Program in Communication Sciences, University of California, Davis, 1544 Newton Ct., Davis, CA 95616 (E-mail: enyamoah@ucdavis.edu).

Moreover, NO further regulates Ca^{2+} channels through NO-mediated activation of protein kinase G.

METHODS

Tissue preparation

The bullfrog saccule was isolated as previously described (Rodriguez-Contreras and Yamoah 2001). The protocol was approved by the University of California, Davis Animal Research Services IACUC committee. Frogs were killed and inner ears were quickly removed and placed in oxygenated low-Ca^{2+} frog Ringer solution (in mM): 110 NaCl, 2 KCl, 3 D-glucose, and 0.1 $CaCl_2$. The saccular macula was isolated and incubated in frog saline containing 50 μg/ml protease (type XXIV; Sigma, St. Louis, MO) for 20 min. The tissue was then washed and transferred to frog saline containing 1 mg/ml bovine serum albumin (BSA; Sigma) and 2 mg/ml DNAse I (Worthington, Lakewood, NJ) for 10 min. The otolithic membrane was excised and the sensory epithelium placed in a recording chamber using cell Tak to secure the tissue at the bottom of the chamber. For experiments in which isolated cells were required, the macular tight junctions in the saccule were disrupted by exposing the perilymphatic surface to 4 mM ethylene glycol-bis(β-aminoethyl ether)-*N*,*N*,*N*′,*N*′-tetraacetic acid (EGTA) for 15 min. After washing the preparation with fresh saline, the saccular macula was isolated and incubated in frog saline containing 50 μg/ml protease (type XXIV; Sigma) for 20 min. The tissue was then washed and transferred to frog saline containing 1 mg/ml BSA and 2 mg/ml DNAse I for 10 min. This procedure has been used previously (Chabbert 1997) and differs from more severe enzymatic treatments that can alter ionic conductances (Armstrong and Roberts 1998). The otolithic membrane was excised and hair cells were dissociated from the macula by use of an eyelash. Hair cells were allowed to settle onto the bottom of the recording chamber (coated with lectin concavalin-A) for 20 min prior to patch-clamp recording.

Preparation of NO microsensors

Carbon fiber electrodes were constructed as previously described (Kumar et al. 2001; Porterfield et al. 2001), by inserting a 5 μm carbon fiber (Amoco, Greenville, SC) through a borosilicate glass pipette (OD 1.5 mm; ID 0.86 mm; World Precision Instruments, Sarasota, FL), using acetone as a lubricant. The electrode was dried at 110°C for 10 min and then pulled using a horizontal puller (P97; Sutter Instrument, Novato, CA). The fiber was retained and sealed within the pulled pipette with Epoxylite (Epoxylite, Westerville, OH) and cured at 110°C for 4 h. Once the epoxylite had cured, the electrode was backfilled with graphite-epoxy paste (PX-grade Graphpoxy; Dylon Industries, Cleveland, OH). To establish electrical contact between the carbon fiber and a preamplifier, a copper wire (diameter: ~700 μm) was inserted into the glass electrode in contact with the graphite-epoxy paste. The graphite-epoxy was polymerized at 110°C overnight. The tip of the carbon fiber was trimmed and beveled at a 30° angle and a final tip diameter of about 2–3 μm was obtained. To make the electrode selective for the oxidation of NO, the carbon fiber was modified using the procedure described (Friedemann et al. 1996). The carbon fiber was coated with Nafion (5% in aliphatic alcohol; Aldrich, Milwaukee, WI) and *o*-phenylenediamine (o-PD; Sigma). Nafion is a polysulfonated Teflon that carries negative charge and repels electrochemically active anions (e.g., nitrate, nitrite, and ascorbate). o-PD confers selectivity to NO oxidation by size exclusion of noncharged interferents such as electrochemically active catecholamines. First, the carbon fiber was coated with Nafion and dried at 110°C for 10 min and, using this procedure, was repeated twice. Next, the Nafion-coated carbon fiber was plated with a 5 mM o-PD plating solution consisting of 0.1 mM ascorbic acid in 100 mM phosphate buffer saline (PBS, pH 7.4). The plating voltage was a constant +0.9 V applied until desirable noise characteristic was obtained. The NO-selective electrode was operated with an Ag/AgCl return electrode that completed the circuit in solution though a 3 M KCl/3% agar bridge. The polarization voltage used was 0.9 V and the electrode was operated in self-referencing mode, as described for self-referencing NO and O_2 electrodes (Kumar et al. 2001; Land et al. 1999).

Calibration of NO electrodes

A stock of saturated NO solution was prepared fresh daily. First, frog saline was made O_2-free by bubbling the solution in a vacuum-sealed container with O_2-free argon for 45 min. The solution was then bubbled with NO gas for 30 min. The pH of the solution was adjusted to 7.4. The concentration of NO obtained using this protocol was about 2 mM (Ahmmed et al. 2001; Friedemann et al. 1996). The stock solution was diluted into several series and the sensitivity of the electrode tested. Five electrodes were constructed and their sensitivity for NO was 0.77 ± 0.15 pA/μM (n = 5). In contrast, the sensitivity of the electrodes to sodium nitrite was roughly 600-fold less than that to NO (sensitivity for nitrites was 1.28 pA/mM). Despite the variations in the sensitivity of the electrodes, they responded well to changes in NO concentrations in a linear fashion (Porterfield et al. 2001; see Fig. 1). To reduce inherent drifts associated with polarographic electrodes and to increase the sensitivity of the NO electrodes, the electrodes were used in a self-referencing mode (Smith et al. 1999). Using the release of NO from *S*-nitroso-*N*-acetylpenicillamine (SNAP) in a source micropipette to test for the sensitivity of the NO electrodes, we measured the gradient generated by the source (10 mM SNAP in PBS in ~10 μm diameter micropipette) and thus established that the NO selective electrodes were true detectors of NO flux (Porterfield et al. 2001; Shafer et al. 1998; Fig. 1).

Measurements of NO fluxes were performed using the intact saccular epithelium. The tissue was placed on a Zeiss and/or Olympus (BX50WI) upright microscope fitted with a stage plate on which the head stage and translational motion control system were mounted. Motion control allows nanometer resolution of movement of the head stage using square translation steps at 0.3 Hz and in static mode (Smith et al. 1999). The amplifier, motion control, and data acquisition were run with custom-written software (IonView, BioCurrent Research Center, Woods Hole, MA). Data were collected at a rate of 1,000 events/s and signal-averaged to 10 values consisting of 166 data points/position. Values obtained over the period of electrode movement were excluded (first third discarded).

Whole cell recordings

Recordings were performed using an Axopatch 200B patch clamp amplifier (Molecular Devices, Union City, CA) interfaced to a personal computer. Voltage and current commands were generated and data collected using custom-written software. Patch pipettes were fabricated from borosilicate glass capillaries (World Precision Instruments) on a four-step horizontal Flaming-Brown microelectrode puller (Sutter Instrument) and coated with Sylgard 184 (Dow-Corning, Midland, MI) to within 100 μm of the tip and fire-polished before use. To record Ca^{2+} currents, outward K^+ currents were blocked with tetraethylammonium chloride (TEA-Cl), 4-aminopyridine (4-AP), and cesium (Cs^+) ions. Bath solution contained (in mM) 90 NaCl, 25 TEA-Cl, 5 4-AP, 5 $CaCl_2$, 3 glucose, and 5 HEPES (pH 7.4). Whole cell Ca^{2+} currents were recorded using perforated patch electrodes (resistances 2–4 MΩ) to minimize washout of intracellular molecules. The tips of electrodes were filled with a solution containing (in mM) 130 CsCl and 5 HEPES (pH 7.3 with CsOH). To gain electrical access to the cell, electrodes were backfilled with solution containing (in mM) 130 CsCl, 1 $CaCl_2$, 5 HEPES, and amphotericin 200 μg/ml (pH 7.3 with CsOH) (Korn et al. 1991). To ensure that recordings were in the perforated-patch mode instead of whole cell mode, the backfilled solution of the patch electrode contained 1 mM Ca^{2+}. A switch from

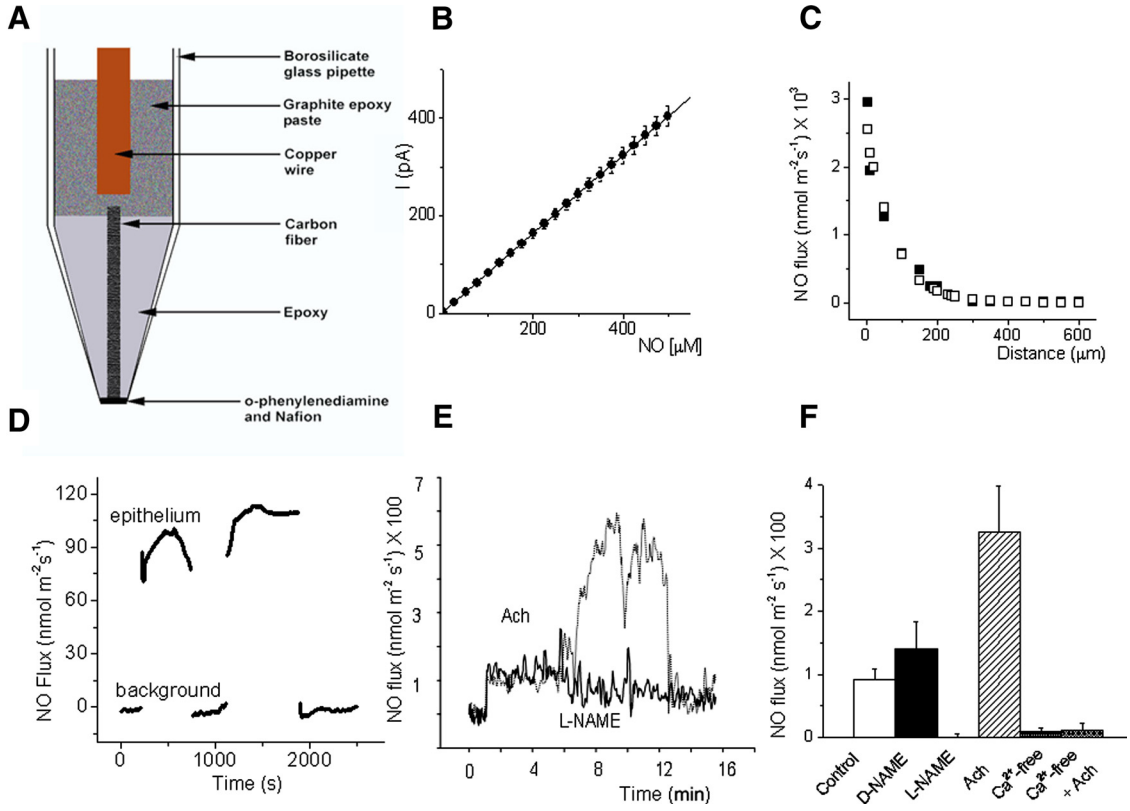

FIG. 1. Measurement of nitric oxide (NO) efflux. *A*: schematic diagram of the NO-sensitive microsensor. The microsensor was constructed by inserting 5-μm carbon fiber and then heating and pulling the glass electrode. Epoxy was backfilled into the electrode to seal the fiber with the glass electrode. A graphite paste was used to cement a copper wire to the carbon fiber. The tip of the electrode was beveled, coated with Nafion, and plated with *o*-phenylenediamine. *B*: the electrodes were calibrated with 21 standards with known concentrations of NO and the selectivity was tested against ascorbic acid. The gradient of the linear regression of the calibration line was used to calculate the flux of NO. *C*: NO flux in relation to the distance from a source pipette (diameter ~3 μm). Symbols represent measured values and the solid squares (■) represent the product of a theoretical model developed from the Fick equation. *D*: data collected from a frog saccule. The excursion distance of the microsensor was 5 μm at a frequency of 0.3 Hz. When in the "epithelium" position the electrode was about 2 μm from the tissue. Background represents data collected at a position 2,000 μm away from the saccule. The mean NO flux was 115 ± 20 nmol·m^{-2}·s^{-1} (n = 15), compared with background reading 1 ± 8 nmol·m^{-2}·s^{-1} (n = 15). *E*: representative recording from a saccule (dotted line) and on application of 5 μM acetylcholine (ACh). Superimposed on the same plot (solid line) is a depiction of the inhibitory effects of N^G-nitro-L-arginine methyl ester (L-NAME). *F*: summary data on the effects of N^G-nitro-D-arginine methyl ester (D-NAME; n = 7), L-NAME (n = 8), ACh (n = 9), Ca^{2+}-free solution (n = 5), and Ca^{2+}-free + ACh (n = 7) on NO efflux.

the perforated to whole cell mode resulted in cell death because of Ca^{2+} toxicity. Series resistance (5–10 MΩ) was compensated (nominally 50–60%). Liquid-junction potentials were <2 mV and were not corrected. Ca^{2+} current records were amplified and filtered at 2–5 kHz with a low-pass Bessel filter and digitized at 10 kHz with a Digidata interface (Axon Instruments) controlled by custom-written software.

To record whole cell K^+ currents, the pipettes were filled with a solution containing (in mM): 130 KCl, 0.1 $CaCl_2$, 5 MgATP, 1–5 EGTA, 10 HEPES, and 1 Na_3GTP, with a pH of 7.3 The external solution was (in mM): 3 KCl, 2 $CaCl_2$, 120 NaCl, 5 HEPES, and/or 5 4-AP, 2.5 TEA, pH 7.4 (NaOH). Data were stored on a personal computer. All experiments were performed at room temperature (~21°C). The capacitance of the cell was calculated by integrating the area under an uncompensated capacitive-transient, elicited by a 20 mV hyperpolarizing pulse from a holding potential of −80 mV.

Single-channel recordings

The standard configurations for cell-attached single-channel of the patch-clamp techniques (Hamill et al. 1981) were used to record Ca^{2+}/K^+ channel currents from hair cells isolated from the bullfrog saccule. Quartz electrodes were pulled with a laser puller (P2000; Sutter Instrument). Single-channel recordings of membrane patches were held at −70 or −60 mV, and stepped to different depolarizing test pulses at frequencies between 0.2 and 0.5 Hz. Current traces were amplified and filtered using an eight-pole Bessel filter at 2 kHz and digitized at 10 kHz using custom-written software. Patch electrodes were filled with a Ca^{2+} solution (50–70 mM) containing (in mM) 20 TEA-Cl, 5 4-AP, and 5 HEPES at pH 7.4 (adjusted with TEA-OH). *N*-Methyl-D-glucamine (NMG) was used to substitute for divalent Ca^{2+} and to maintain an osmolarity of about 280 mmosmol. Stock solutions of 3-pyridinecarboxylic acid-1,4-dihydro-2,6-dimethyl-5-nitro-4-(2-(trifluoromethyl)phenyl)methyl ester (Bay K 8644, 100 mM) were made in DMSO and a final concentration of 5 μM was used. The bath solution contained (mM) 80 KCl, 3 D-glucose, 20 TEA-Cl, 1 $CaCl_2$, 5 4-AP, and 5 HEPES pH 7.4 with TEA-OH, to shift the resting potential to about 0 mV (Rodriguez-Contreras and Yamoah 2003). For Ca^{2+}-activated K^+ channel currents, the bath solution contained (in mM) 110 KCl, 2 $CaCl_2$, 5 4-AP, and 5 HEPES (pH 7.4 with KOH/HCl). The pipettes were filled with a solution containing (in mM): 110 KCl, 5 4-AP, 0.1 $CaCl_2$, 10 HEPES, and 10 glucose (pH 7.3). In all cases, liquid-junction potentials were measured and corrected as described previously (Rodriguez-Contreras et al. 2002). All experiments were carried out at room temperature (~21°C).

Chemicals and solutions

Several chemicals were used. These include N^G-nitro-L-arginine methyl ester and N^G-nitro-D-arginine methyl ester (L-NAME and

D-NAME, respectively; Sigma), dithiothreitol (DTT), a thiol reducing reagent, sodium nitroprusside (SNP, Sigma), 3-morpholinosydnonimine (SIN-1, Molecular Probes, Eugene, OR), and *S*-nitroso-*N*-acetylpenicillamine (SNAP, Molecular Probes), NO donors. All other chemicals were obtained from Sigma, unless otherwise noted.

Data analysis

Whole cell current amplitudes at varying test potentials were measured at the peak and steady-state levels using a peak and steady-state detection routine. For single-channel records, leakage and capacitative transient currents were subtracted by fitting a smooth template to null traces. Leak-subtracted current recordings were idealized using a half-height criterion (Colquhoun and Sigworth 1985). Transitions between closed and open levels were determined by using a threshold detection algorithm, which required that two data points exist above the half mean amplitude of the single-unit opening. The computer-detected openings were confirmed by visual inspection and sweeps with excessive noise were discarded. Amplitude histograms at a given test potential were generated and then fitted to a single Gaussian distribution using a Levenberg–Marquardt algorithm to obtain the mean and SD. At least five voltage steps and their corresponding single-channel currents were used to determine the unitary conductance. Single-channel current–voltage (*I–V*) relations were fitted by linear least-square regression lines and single-channel conductances obtained from the slope of the regression lines. Idealized records were used to construct ensemble-averaged currents, open probability, and histograms for the distributions of open and closed intervals. Curve fits and data analyses were performed using Origin software (MicroCal, Northampton, MA). Where appropriate, pooled data are presented as means ± SD.

RESULTS

Release of NO by the frog saccule

Using a variety of direct and indirect immunoreactive techniques, it has been established that the vestibular maculae and cochlea of vertebrates show distinct expression of nitric oxide synthase (NOS; Fessenden and Schacht 1998; Lysakowski and Singer 2000; Michel et al. 1999; Riemann and Reuss 1999; Singer and Lysakowski 1996). To determine the functional significance of activation of NOS, we first characterized and quantified NO production in the frog saccule using the self-referencing amperometric probe technique (Fig. 1*A*). Figure 1*B* illustrates experiments performed to examine the sensitivity of five NO-selective electrodes and to determine the release of NO fluxes from the saccular epithelia. The current generated at the electrode, polarized to 0.9 V, was measured differentially between two points at the background (~2,000 μm) from the sensory epithelia and at the tissue (~2 μm from the tissue). Using the Fick equation as described (Kumar et al. 2001; Land et al. 1999), we calculated NO flux, by measuring the static NO concentrations over a given distance within a gradient established by an artificial source (Fig. 1*C*) and the tissue as a source of NO release. As illustrated in Fig. 1*D*, which shows a representative example of the NO efflux (nmol·m^{-2}·s^{-1}), when the electrode was moved from the background to the saccule, there was an approximately 200-fold change in the NO efflux. Application of frog saline containing L-NAME resulted in gradual attenuation of NO efflux, consistent with the inhibition of NOS. Baseline extrusion of NO from the frog saccule was reliably observed in 15 samples that were tested (115 ± 20 nmol·m^{-2}·s^{-1}, $n = 15$). Moreover, L-NAME inhibited the NO efflux to 2 ± 12 nmol·m^{-2}·s^{-1} ($n = 8$). In contrast, application of the inert enantiomer (D-NAME) produced a mean net efflux of 159 ± 36 nmol·m^{-2}·s^{-1} ($n = 7$), thus suggesting that the NO efflux from the frog saccule was NOS-specific. Next, we examined the effects of ACh on NO efflux from the saccule. As shown in Fig. 1*E*, application of ACh caused a rapid and sustained efflux of NO. The ACh-mediated rise in NO efflux (ACh-induced effects = 324 ± 105 nmol·m^{-2}·s^{-1}, compared with control = 114 ± 27 nmol·m^{-2}·s^{-1}, $n = 9$, $P < 0.05$), was also inhibited by L-NAME, again suggesting the involvement of NOS in the ACh-mediated release of NO. As shown in the summary data (Fig. 1*F*), the ACh-mediated release was dependent on extracellular Ca^{2+}. Replacement of the normal frog saline and application of a Ca^{2+}-free saline, which included the Ca^{2+} cheletor EGTA (5 mM), decreased the baseline NO efflux and attenuated the ACh-induced rise in NO efflux.

NO and NO donors decrease hair-cell membrane excitability

The functional consequences of the release of NO in or at the vicinity of hair-cell membrane properties were examined at the current-clamp recording conditions, using perforated (amphotericin) patches. As illustrated in Fig. 2*A* (*top left*) isolated hair cells in the frog saccule typically exhibit baseline membrane oscillations. Of 56 cells that were sampled, 50 (89%) had spontaneous baseline membrane oscillations, whereas the remaining 6 (11%) were quiescent. Injection of current resulted in increased membrane fluctuations until the characteristic frequency oscillation ensued. Figure 2*A* shows examples of such membrane voltage oscillations. In contrast to recordings from control hair cells, application of SNAP not only attenuated the baseline membrane oscillations, but it also resulted in increased magnitude of the injected current required to generate characteristic membrane potential oscillations (Fig. 2*B*). The resulting effects of NO were to shift the frequency–current relationship to the right, thus altering the excitability of hair cells (Fig. 2*C*). Similar effects were observed with the NO donor SIN (10 μM) and by direct application of NO (100 nM) solution. Within 3 min of application of NO donors/NO solution, the effect was reversed readily by washing the drug with normal frog saline containing about 200 μM of the reducing agent DTT. DDT (200 μM) alone had no effect on membrane potential oscillations (data not shown); however, sustained exposure of hair cells to NO donors/NO (>7 min) resulted in only partial recovery after washout with DTT.

The mechanisms of membrane oscillation in hair cells in lower vertebrates have been ascribed mainly to the interplay between activation of voltage-gated Ca^{2+} currents (VGCCs) and Ca^{2+}-activated K^+ currents (BKs), although the contribution of other voltage-gated K^+ currents in hair cells that are tuned to low frequencies have been reported (Armstrong and Roberts 1998; Art et al. 1993; Fuchs 1992; Fuchs and Evans 1988; Holt et al. 1997; Hudspeth and Lewis 1988b). To determine the underlying mechanisms for the NO-induced changes in hair-cell excitability, we studied the effects of the NO donors SNAP, SNP, and NO on VGCC and BK currents. To record Ca^{2+} currents, outward K^+ currents were blocked with external TEA, 4-AP, and internal Cs^+. Figure 3, *A–C* shows representative traces of Ca^{2+} currents and the effects of NO, dibutyryl-3′,5′-cyclic guanosine monophosphate (cGMP),

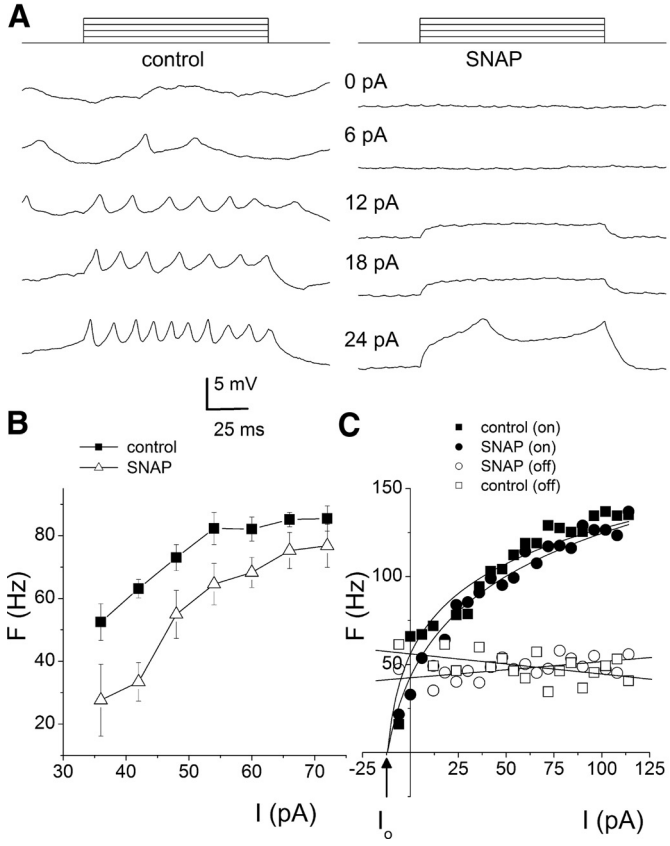

FIG. 2. NO donor *S*-nitroso-*N*-acetylpenicillamine (SNAP) decreases the membrane gain of hair cells. *A*: a family of oscillations of hair-cell membrane potentials in the absence and in response to injection of current steps (indicated) for controls (*left*) and after application of 10 μM SNAP. The NO donor reduces baseline membrane oscillations. *B*: the resulting effects of the NO donor is a shift in the frequency–current (*F–I*) relationship to the *right*. *C*: the frequency of membrane potential oscillations as a function of injected current for a hair cell. The oscillations at current "on" in solid symbols and oscillations at current "off" are in open symbols. The solid curves were calculated using the equation (Crawford and Fettiplace 1981): $F_R(I) = \hat{F} \log_e [1 + \mu(I - I_o)]$, where F_R is the frequency of oscillation at a given current step of amplitude I, I_o is the minimum outward current required to suppress the oscillations, and $\hat{F}$ and μ are constants for the cell with units of Hz and reciprocal current, respectively. For the example shown, the NO donor appears to shift the characteristic frequency of the cell from about 55 to 40 Hz.

and DTT, as well as the *I–V* relation generated by a series of voltage-clamped steps from holding potential of −70 mV. In the presence of NO donors, the whole cell Ca^{2+} current was reduced by 34.0 ± 6.0% by SNAP (n = 11), 31.2 ± 4.1% (n = 9) by SNP, and 35.8 ± 5.3% by NO of the total current (n = 14). NO produced an approximately 3.5 mV rightward shift in the steady-state activation curve (Fig. 3*D*). A concentration–response curve was constructed for NO and a half-blocking concentration of about 80 nM and Hill coefficient of 1 were determined (Fig. 3*E*). Because NO solution is relatively unstable after exposure to atmospheric O_2, we simulated the experimental conditions for the perfusion of NO in the recording chamber and then used the NO-selective electrode to determine the NO concentration that was exposed to hair cells versus the applied concentration. Aside from the reduction of the magnitude of the Ca^{2+} current, NO produced no measurable effect on the kinetics of the current. Moreover, consistent with the current-clamp data, NO produced a two-phased effect: an early DTT-mediated reversible effect and a late DTT-irreversible effect. As illustrated in Fig. 3*B*, cGMP mimicked the late effect of NO and, in the presence of KT-5823 (the specific inhibitor of protein kinase G), DTT fully reversed the actions of NO. The summary data are shown in Fig. 3*F*.

Even though reduction of the inward Ca^{2+} currents could reduce the excitability of hair cells and increase the threshold for the induction of membrane oscillations, enhancement of outward K^+ currents could produce similar outcomes through membrane repolarization. We recorded whole cell K^+ currents and determined that only the Ca^{2+}-dependent component was affected by NO (data not shown). We examined the effects of NO on the Ca^{2+}-activated K^+ (BK) current by blocking the voltage-gated K^+ currents with 4-AP (Armstrong and Roberts 2001; Hudspeth and Lewis 1988a). Figure 4*A* illustrates BK-current traces, which were elicited from a holding potential of −90 mV and stepped to depolarizing potentials (ΔV = 5 mV) recorded in both the absence and the presence of NO and DTT. The BK current was enhanced after application of NO and its effects were reversed by DTT. The *I–V* relationship in Fig. 4*B* provides a summary of the data. The increase in magnitude of the outward current could result from the masking effect of reduction of inward Ca^{2+} current. However, the increase in magnitude of the outward K^+ current was larger than could be ascribed to a reduction of NO-induced block of the Ca^{2+} current alone, suggesting that NO may modulate the BK current as well. We examined this further by subjecting the cells to brief prepulses (~25 ms) to activate the VGCC, followed by a sustained (>500 ms) depolarizing test pulse to activate the BK current. Shown in Fig. 4*C*, the results indicated that NO suppressed the VGCC and enhanced the BK current as well; the effects of NO on the BK current were reversed by DTT. Thus NO-modified ionic currents in hair cells suppress their excitability.

Mechanisms for NO modulations of single Ca^{2+} and BK currents

Hair cells in the frog saccule express multiple Ca^{2+} and BK channels (Armstrong and Roberts 2001; Rodriguez-Contreras and Yamoah 2001; Rodriguez-Contreras et al. 2002). To prevent contamination and masking effects of inward and outward currents at the whole cell current level, a reasonable approach to determine the mechanisms of NO effect is to examine the current at the single-channel level. Figure 5, *A–C* shows single-channel Ca^{2+} currents obtained from a cell-attached patch containing a nimodipine-insensitive channel. The patch pipette contained 65 mM Ca^{2+} and the patch was held at −70 mV and stepped to −50 mV. Because of the pharmacology of the channel and its slow-voltage activation as well as its conductance (16.2 pS; Fig. 5*E*), the channel was classified as a non L-type Ca^{2+} channel (Rodriguez-Contreras and Yamoah 2001). Shown in Fig. 5*D* are examples of amplitude histograms, used to generate the *I–V* relations (Fig. 5*E*). The effect of NO on the probability of the non L-type channel openings (P_o) was robust and reversible by DTT (0.2 mM) (mean P_o values at test potential of −50 mV were: control, 0.18 ± 0.07; after application of NO, 0.07 ± 0.01; and after DTT, 0.20 ± 0.05; n = 9). Similar results were obtained when SNAP (100 μM) was used (mean P_o values at test potential of −50 mV were: control, 0.21 ± 0.05; after application of SNAP, 0.09 ± 0.03; and after DTT, 0.19 ± 0.03; n = 5).

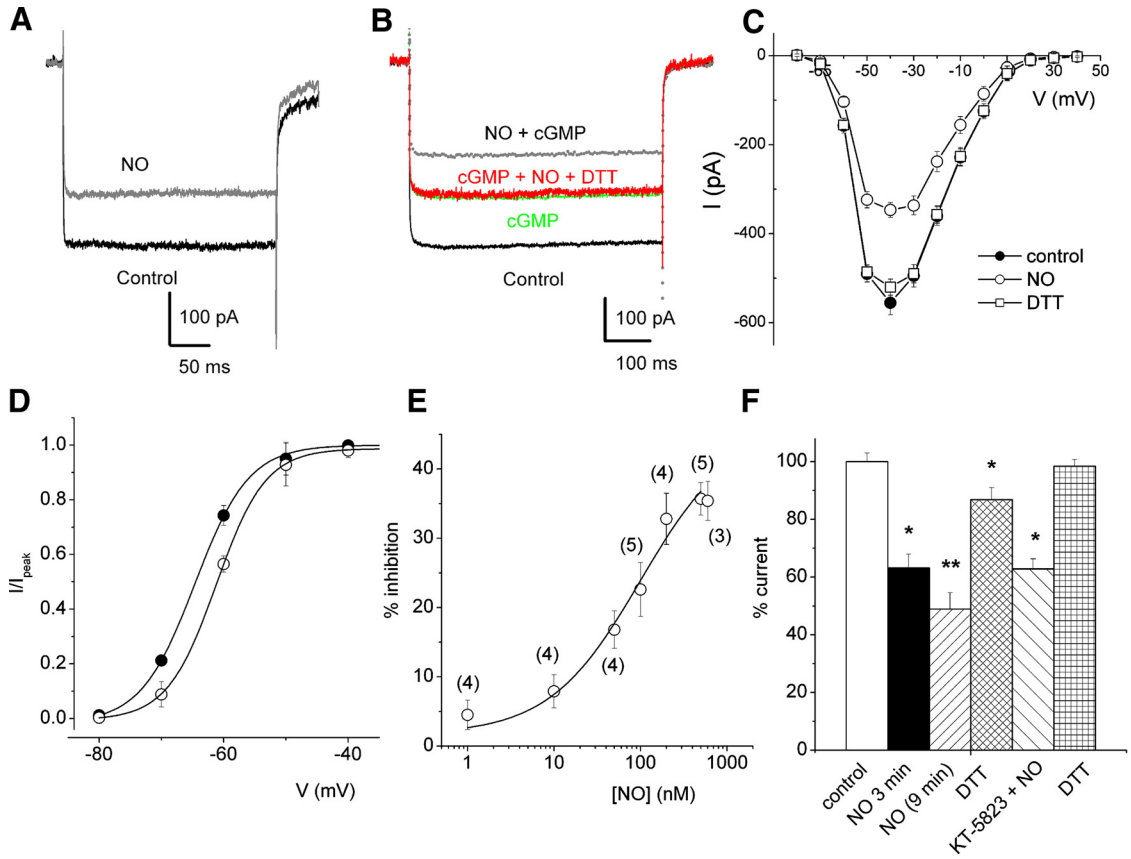

FIG. 3. Effects of NO and activation of protein kinase G (PKG) on inward Ca^{2+} current in hair cells measured using whole cell patch clamp. *A*: current traces obtained by 250-ms depolarization pulses from a holding potential of −70 mV to a step potential of −30 mV in the absence (black trace) and the presence of 500 nM NO (as measured with an NO-selective electrode). *B*: similar recordings were made in the absence, control, and presence of 10 μM dibutyryl-3′,5′-cyclic guanosine monophosphate (cGMP), 10 μM cGMP plus 600 nM NO, and 10 μM cGMP plus 600 nM NO and 1 mM dithiothreitol (DTT). Whereas the effects of NO were reversed by DTT, the effect of cGMP was unaltered by DTT (control = −556 ± 31 pA, cGMP = 389 ± 19 pA; $n = 7$, $P < 0.05$; control = −578 ± 42 pA, cGMP + NO = −274 ± 16 pA; $n = 8$, $P < 0.01$). *C*: representative current–voltage (*I–V*) relations generated from data from 14 cells showing the effects of NO (1 μM) and DTT (1 mM). The peak control Ca^{2+} current, −555 ± 27 pA, was reduced to −347 ± 17 pA ($n = 14$, $P < 0.01$) by NO after 3 min exposure. The effects of NO was reversed by application of 1 mM DTT (−519 ± 18 pA; $n = 14$ $P = 0.08$). *D*: steady-state activation curves were generated using the ratio of the tail currents (I/I_{peak}) against the step potentials. The continuous curves were generated from the Boltzmann function $\{I/I_{peak} = [1 + \exp(V_{1/2} - V)/K_m]\}^{-1}$. $V_{1/2}$ is the half-activation voltage and K_m is the slope factor. The estimated values of $V_{1/2}$ and K_m for control currents (●) and currents after application of NO (○) were (in mV): −64.6 ± 0.5 and 4.3 ± 0.5; and −61.2 + 0.6 and 4.1 ± 1.0 ($n = 8$ cells), respectively. *E*: NO inhibition of Ca^{2+} current was dose dependent. The half-blocking concentration of NO was estimated to be 81 ± 7 nM ($n = 4$). *F*: group data showing the effects of NO after 3 min ($n = 8$) and 9 min ($n = 6$) application, DTT ($n = 6$) on NO-mediated effects, actions of NO in the presence of KT-5823 ($n = 7$), a PKG inhibitor, and the effects of DTT on the actions of NO in the presence of the PKG inhibitor ($n = 5$; *$P <$ 0.05; **$P < 0.01$).

As depicted in Fig. 6, NO produced a modest decline in the P_o of the L-type channel, compared with that of the non L-type channel. The single L-type Ca^{2+} channel fluctuations recorded from hair cells in the cell-attached configurations were reduced by application of NO (500 nM) and SNAP (100 μM). Examples of the L-type Ca^{2+} channel currents traces recorded from a holding potential of −70 mV and step potential of −30 mV are shown in Fig. 6, *A–C*. The *I–V* relation shown in Fig. 6*E* was generated using unitary current magnitudes derived from the amplitude histograms (Fig. 6*D*). The conductance of the channel (13.6 pS) and its sensitivity to Bay K 8644 (the dihydropyridine agonist) suggests that the channel belongs to the L-class of Ca^{2+} channels. As shown in the diary plot in Fig. 6*F*, the application of 1 μM NO reduced the P_o of the L-type channel. Moreover, the extent of reduction of the P_o by NO and SNAP was similar (control P_o: 0.16 ± 0.06; NO: 0.07 ± 0.02 $n = 7$; $P < 0.01$; control P_o: 0.14 ± 0.09; SNAP: 0.04 ± 0.01 $n = 6$; $P < 0.01$) and was reversed partially by DTT (after DTT P_o: 0.11 ± 0.02 ($n = 7$) and 0.09 ± 0.03 ($n = 6$) NO and SNAP, respectively. In contrast to the non L-type channel, which was reversed readily by DTT even after 20 min of application of NO, the effect of NO on the L-type channel was irreversible after 10 min exposure to NO. The differential effects of NO on the non L and L-type channels can be noticed in patches containing two channel subtypes (Fig. 7). Thus NO-induced reduction of the macroscopic Ca^{2+} current is derived from diminution of the P_o at the unitary channel level.

Open times were abbreviated in NO-modified Ca^{2+} channels. Open times were fitted by using bi- or triexponential functions for both patches. Compared with the control in Fig. 8, time constants obtained from NO-modified patches were significantly abbreviated by exposure to 100 nM NO [e.g., 2.2 ± 0.01 ms (control) vs. 0.50 ± 0.02 ms ($n = 4$; $P < 0.05$)] in NO-modified patches, respectively. DTT (0.2 mM) restored the fast open-time constant (1.1 ± 1.5; $n = 3$; $P = 0.7$). Also important, the fast open-time constant was eliminated in NO-modified L-type single-channel current kinetics.

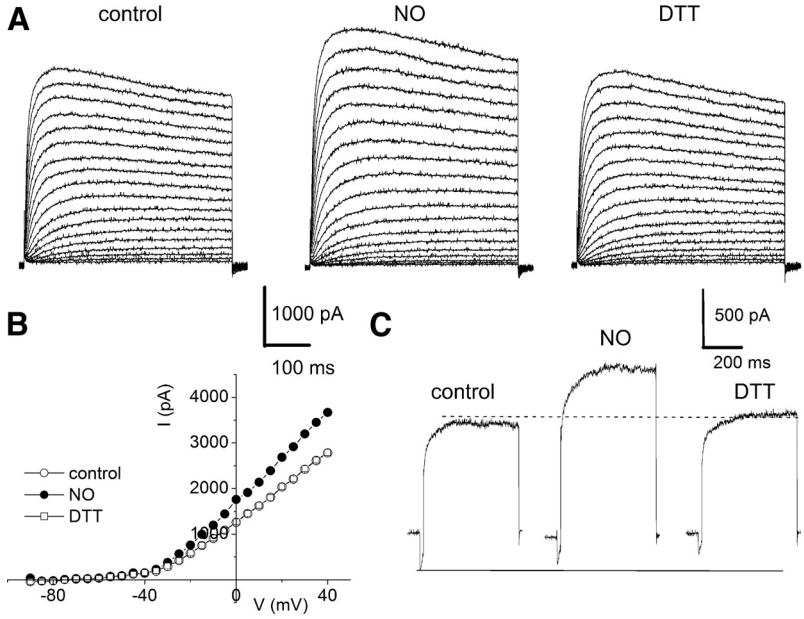

FIG. 4. Whole cell recordings of Ca^{2+}-activated K^+ current in hair cells. The amplitude of outward Ca^{2+}-activated K^+ currents was increased by NO. *A*: outward K^+ currents traces were elicited at a holding potential (−90 mV), step depolarization of −80 to 40 mV, with change in voltage of 5 mV. The current was recorded in the presence of 5 mM 4-aminopyridine (4-AP) and tetraethylammonium (TEA) to suppress other outward K^+ currents (see METHODS). The current was enhanced in response to increased external Ca^{2+} (data not shown). The Ca^{2+}-activated K^+ currents were visibly enhanced on application of NO (600 nM) and the effect was reversed by 1 mM DTT. *B*: the summary data (n = 9) of the *I–V* relationship for data obtained from control experiments (○), after application of NO (●), and reversal effects of 0.2 mM DTT (□). *C*: to confirm the enhancement effect of NO on the Ca^{2+}-activated K^+ current, hair cells were held at −70 mV and stepped briefly (25 ms) to −30 mV to activate the inward Ca^{2+} current and then stepped to 5 mV to activated the outward K^+ current (n = 5). The increase in the outward current was independent of the reduction of inward current. DTT completely reversed the effect of NO on the K^+ current but not the Ca^{2+} current.

The activity of single BK channels was recorded in the cell-attached mode with patch pipettes containing 110 mM K^+. Similar to previous reports (Armstrong and Roberts 1998; Art et al. 1995; Hudspeth and Lewis 1988a; Roberts et al. 1990), a large conductance (BK) channel with unitary current magnitude of about 7 pA at a step potential of 20 mV was recorded from hair cells. Shown in Fig. 9*A* are exemplary consecutive current traces recorded from a holding potential of −50 mV and at step potential of 20 mV. Amplitude histograms were generated to determine the unitary current amplitudes (e.g., Fig. 9*C*). The corresponding unitary *I–V* relations yielded a conductance of 275 ± 6 pS (n = 7: Fig. 9*D*). In contrast to the effects of NO on the Ca^{2+} channels, application of NO to the BK channel resulted in a substantial increase in P_o of the channel (Fig. 9*B*). The diary plot of the P_o illustrates the pronounced effects of NO compared with control and the recovery that ensues after application of DTT (Fig. 9*E*). However, the unitary conductance remains unchanged in both the presence and the absence of NO and DTT.

DISCUSSION

This study provides the first direct evidence to demonstrate that the sensory epithelia of the frog saccule release NO, which is enhanced by ACh in a Ca^{2+}-dependent manner. The electrophysiological consequences of the release of NO are a

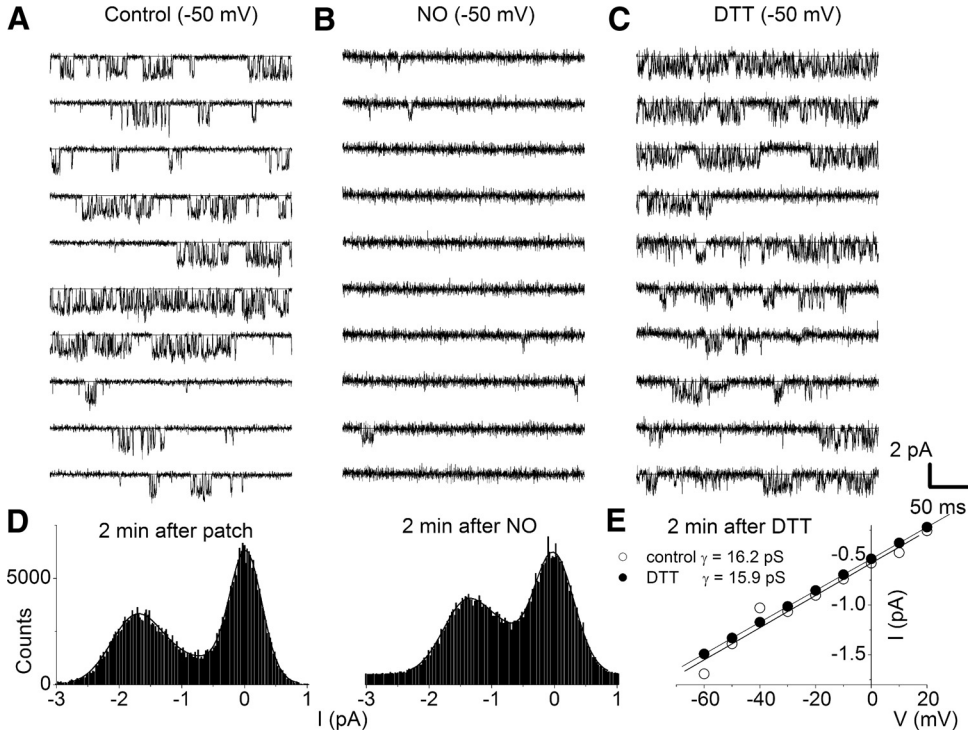

FIG. 5. Single-channel Ca^{2+} current fluctuations in hair cells plummeted in NO but the effect was reversed by DTT. Representative single-channel traces recorded using 65 mM Ca^{2+} as the charge carrier of (*A*) control, (*B*) 2 min after application of 500 nM NO, and (*C*) 2 min after application of 0.2 mM DTT. The recordings were made in bath and pipette solutions containing 10 μM nimodipine. Ten consecutive traces are shown at the step potential indicated (−50 mV) from a holding potential of −70 mV. *D*: examples of amplitude histograms (step voltage, −50 mV) used to generate the *I–V* relationships for control (*left*) and after DTT (*right*). *E*: the *I–V* relationship of control (○) and after DTT (●). The single-channel conductances were: control, 16.2 ± 0.8 pS (n = 6) and after DTT, 15.8 ± 1.3 pS (n = 5) (P = 0.6). The insensitivity of the channel to nimodipine and the conductance suggests that it belongs to the non L-type Ca^{2+} channel subtype (Rodriguez-Contreras and Yamoah 2001).

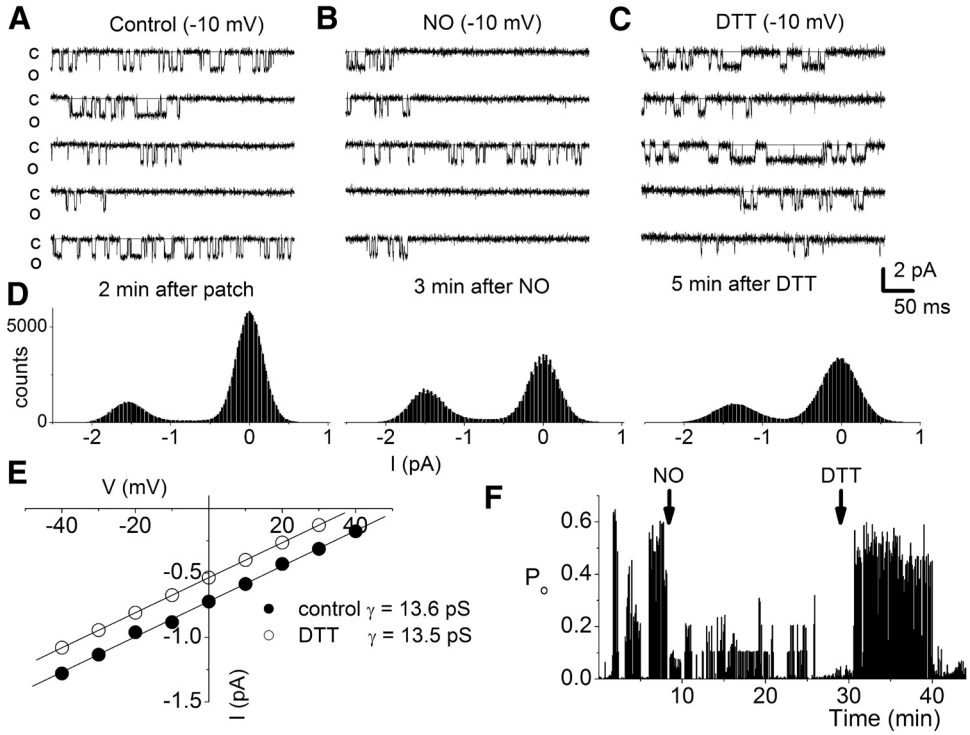

FIG. 6. NO reduces the open probability of L-type Ca^{2+} channel in hair cells. *A–C*: recordings showing effects of NO modification on single-channel Ca^{2+} current from a cell-attached patch during baseline (*A*) and after 3 min of superfusion with external solution containing 500 nM NO (*B*), and finally after application of external solution with 1 mM DTT (*C*). Recordings were obtained using 400-ms steps to −10 mV from a holding potential of −70 mV. Bay K 8644 (5 μM) was included in the patch pipette. *D*: amplitude histograms of the unitary current at −10 mV in control (*left*), the presence of NO (*middle*), and after application of DTT (*right*). *E*: graph showing single-channel *I–V* relations obtained from control patches (●, $n = 5$), NO (○, $n = 5$), and DTT-modified (□, $n = 5$) patches. The calculated conductances were 13.5 ± 0.7, 13.2 ± 0.8, and 13.6 ± 0.3 pS for control, NO, and DTT-modified patches, respectively. *F*: diary plot of open probability vs. time during control, after superfusion with NO-containing solution, and after application of DTT.

profound suppression of the baseline membrane oscillation and a reduction in membrane excitability in hair cells. The elementary mechanisms for NO-induced effects are derived from NO inhibition of the non L- and L-type Ca^{2+} channels by attenuation of the P_o. Moreover, NO inhibited non L-type Ca^{2+} channels and exhibited a sparse pattern of opening, which is reversed through redox modulation with DTT. Additionally, the inhibitory effect of NO on Ca^{2+} channels is augmented by the enhanced activity (P_o) of the large conductance BK channels in hair cells. Since activation of voltage-gated Ca^{2+} channels in hair cells occurs at hyperpolarized potentials (~ −50 mV), and specifically the P_o of the non L-type channels is substantial at rest (Rodriguez-Contreras and Yamoah 2001), NO inhibited Ca^{2+} channels and activated BK channels promote reduction of the membrane excitability of hair cells, resulting in an increase in the threshold of activation. Our findings provide the underlying elementary mechanism for the effects of NO on hair cells and help to clarify universal and divergent viewpoints of previous studies on NO-mediated actions (Almanza et al. 2007; Chen and Eatock 2000; Vega et al. 2006). Moreover, the results raise new possibilities regarding differential modulation of ionic currents in diverse tissues in the inner ear, but with a common theme of altering the electrical gain in hair cells.

We have demonstrated that sulfhydryl modification of L and non L-type channels in hair cells results in a reduction in whole cell Ca^{2+} currents, which is readily reversed by disulfide reduction. At the unitary current level, the decline in macro-

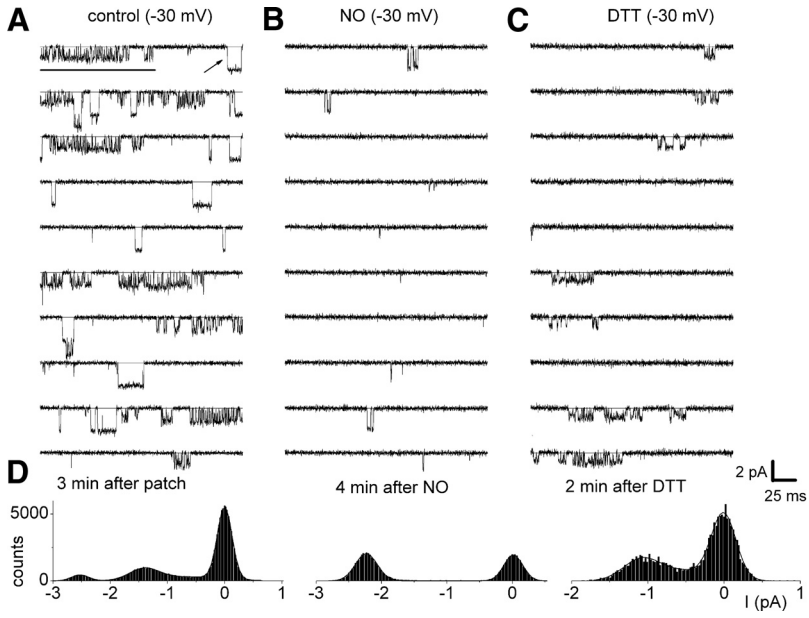

FIG. 7. Differential effects of NO and DTT on L- and non L-type Ca^{2+} channels in hair cells. *A*: family of consecutive single channel fluctuations recorded in a cell-attached patch (charge carrier was 65 mM Ca^{2+}). The patch contained 2 distinct single channels, one with openings suggestive of L-type channel (arrow) and the other, the non L-type channel (underlined). The bath and patch electrode contained Bay K 8644 (5 μM). Ten consecutive traces shown were generated from a holding potential of −70 mV to a step potential of −30 mV. *B*: after superfusion of bath solution containing 500 nM NO, openings of the channel with the non L-type channel were dramatically reduced. However, brief openings of the L-type channel persisted. *C*: on application of DTT (0.2 mM), a substantial number of openings of the non L-type channel emerged. *D*: amplitude histograms of the corresponding unitary current for control (*left*), in the presence of NO (*middle*), and DTT (*right*).

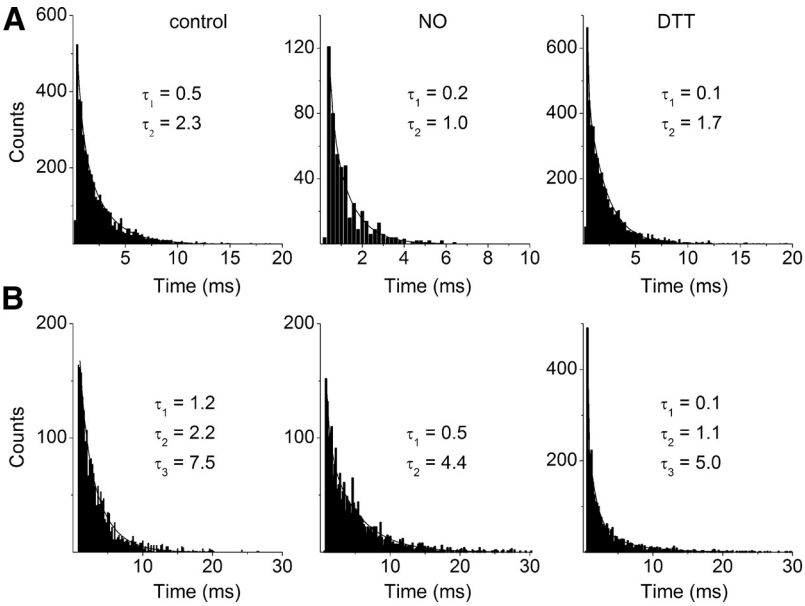

FIG. 8. Effects of NO modification on single-channel Ca^{2+} current kinetics. Currents were obtained from control, NO-modified (100 nM), and DTT-modified (0.5 mM) patches during 400-ms steps to −30 mV (*A*) and −10 mV (*B*) from a holding potential of −70 mV. *A*: open-time histogram plotted as the complement of the distribution. The solid line represents a biexponential fit to the data, with time constants indicated on the plots. The bath solution and pipette contained 10 μM nimodipine and the kinetics and conductance of the channel suggested that it belonged to the non L-subclass. At least one open-time constant was abbreviated in the presence of NO. *B*: here, Bay K 8644 (5 μM) was included in the bath and the pipette. Plots of open-time distribution in the control (*left*), NO-modified (*middle*), and DTT-modified (*right*) L-type channels are shown. The solid lines represent bi- and triexponential fits to the data, with time constants indicated on the plots. Compared with control, time constants obtained from NO-modified patches were significantly abbreviated by exposure to 100 nM NO [e.g., 2.2 ± 0.01 ms (control) vs. 0.50 ± 0.02 ms ($n = 4$; $P < 0.05$) in NO-modified patches, respectively]. Note that DTT (0.2 mM) restored the fast open-time constant (1.1 ± 1.5; $n = 3$; $P = 0.7$). Also important, the fast open-time constant was eliminated in NO-modified L-type single channel current kinetics.

scopic current was mediated by a decrease in P_o and open time, with no change in unitary channel conductance, in agreement with changes in gating but not permeation of Ca^{2+} channels. However, prolonged exposure of NO to hair cells induces further inhibition of Ca^{2+} currents by activation of a cGMP-signaling pathway. These inhibitory effects of NO and/or NO donors on Ca^{2+} currents cannot be reversed by sulfhydryl-reducing agents after prolonged exposure, as would be expected for a direct modulation. In support of this assertion, we showed that the second component of inhibition of the whole cell Ca^{2+} current was abolished by KT-5823, a protein kinase G inhibitor. Additionally, dibutyryl-cGMP produces a reduction of the Ca^{2+} current and, in the presence of the cGMP analog, NO induces a single component of the current inhibition. Consistent with previous reports from hair cells in rat semicircular canals and cardiac cells (Almanza et al. 2007; Campbell et al. 1996), the data suggest that hair-cell Ca^{2+} current can be modulated by both direct (S-nitrosylation/oxidation) and indirect (cGMP-dependent) pathways. The present experiments also demonstrate the presence of constitutive NOS in hair cells and reveal a NO-mediated cholinergic response that, until now, has not been realized in the auditory and vestibular settings. In contrast, it has been established that cholinergic modulation of heart rate is mediated by the release of NO in cardiac cells (Han et al. 1998). The Ca^{2+} dependence of ACh action on release of NO is in keeping with the requirement for Ca^{2+}-mediated calmodulin activation of NOS (Chvanov et al. 2006; Song et al. 2008), in that the Ca^{2+} chelators EGTA/BAPTA attenuate the ACh-mediated effects (Han et al. 1998). Moreover, it can be inferred from our data that the source of Ca^{2+} may be derived in part from influx through hair-cell Ca^{2+} channels.

For the large conductance potassium current, the actions of NO may involve direct nitrosylation of the channel since the reducing agent DTT reversed the inhibitory effects of NO on whole cell and single-channel currents. Similar to Ca^{2+} channel activity, the direct effects of NO on the BK channels is derived from alterations in the P_o; findings that are akin to a previous report on NO-induced activation of BK channels in mesenteric and spiral modiolar arteries (Jiang et al. 2004; Mistry and Garland 1998). By increasing BK channel and reducing Ca^{2+} channel activities, the net effect will promote membrane hyperpolarization and reduction in excitability in accord with the NO-mediated actions on rat vestibular hair cells (Almanza et al. 2007). However, the complexity of the actions of NO cannot be underestimated since it has an inhibitory effect on a large conductance voltage-activated K^+ current in type I vestibular hair cells, $I_{K,L}$ (Chen and Eatock 2000), which is expected to increase the electrical gain of hair cells. Thus the resultant effects of NO actions may depend on the composition and magnitude of ionic conductances relative to the total membrane conductance in a given hair cell.

NO is released as a second messenger that exerts many of its actions by way of several interrelated redox forms to produce direct and distinct features and reactivities on proteins. The by-products of NO consist of nitrogen (N)-oxides, which exhibit reactivity profiles that are distinct from NO itself (Ahmmed et al. 2001; Stamler et al. 1992). Indeed, it has been demonstrated that the regulation of protein functions by alteration of the redox state through reactions of vicinal thiols, which serve as allosteric modulators of ion channels (Ruppersberg et al. 1991). A second level of NO-mediated effects is through an indirect pathway involving activation of adenylyl and guanylyl cyclase and increased levels of cGMP (Ahmmed et al. 2001). Consequently, there is an ensuing activation of protein kinases and phosphorylation of ion channels, resulting in regulation of their functions. These NO-mediated effects have been found to govern a series of biological mechanisms including vasodilation, neurotransmission, and neuronal plasticity (Snyder 1992; Snyder and Bredt 1992). A series of reports have shown high levels of expression of NOS in the cochlea and vestibular end organs (Fessenden and Schacht 1998; Fessenden et al. 1994; Gosepath et al. 1997; Lysakowski and Singer 2000). Additionally, it has been reported that NO donors suppress cochlear potential and outer hair-cell responses (Chen et al. 1995). Using electrochemical and fluorescence detection methods of NO, Shi et al. (2002) measured increased levels of NO in the cochlea after noise exposure (Shi

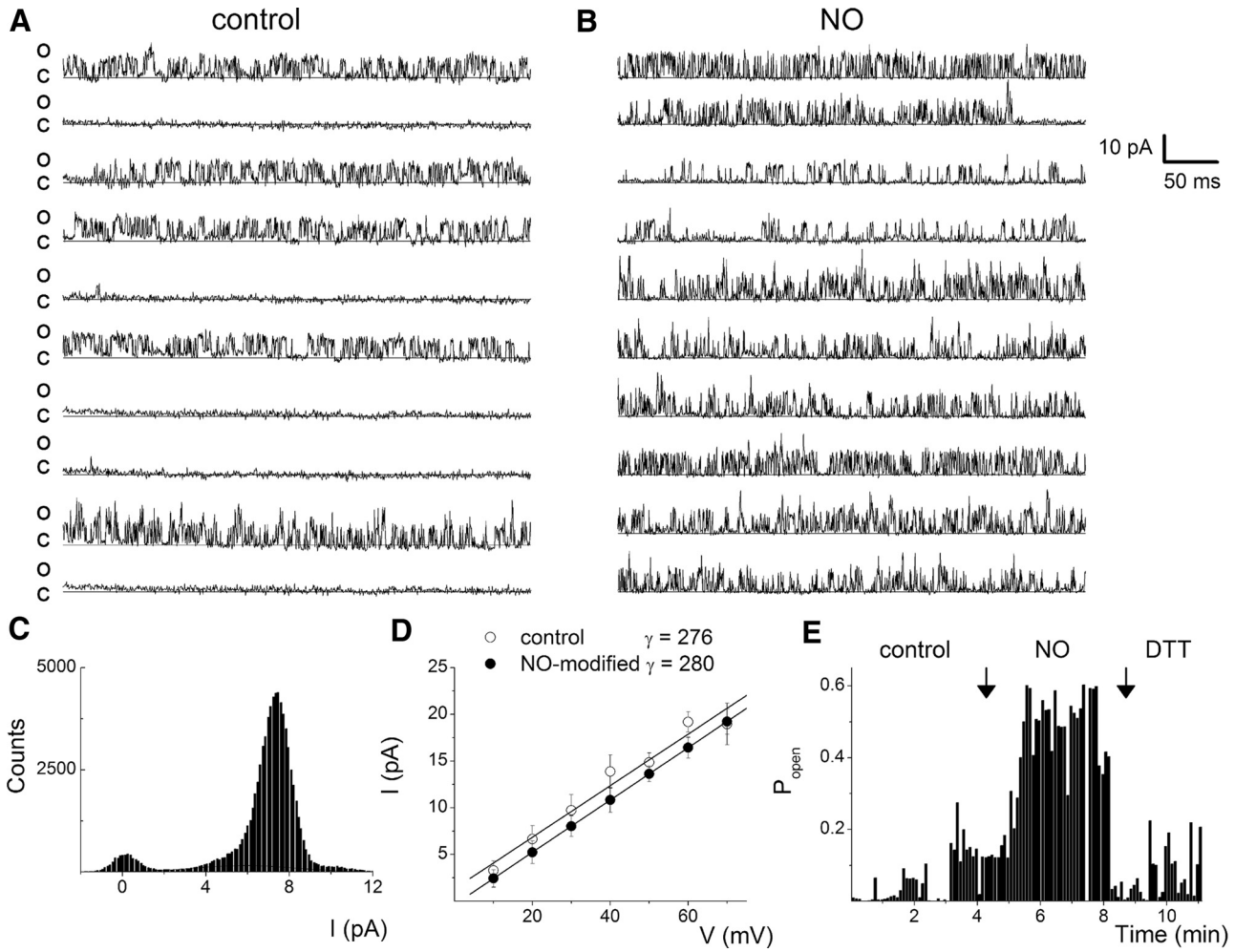

FIG. 9. NO modulates the large conductance single-channel K^+ current in hair cells. *A* and *B*: recordings showing effects of NO modification on single-channel BK channel current from a cell-attached patch during baseline (*A*) and after 2 min of superfusion with 100 nM NO (*B*). Recordings were obtained using approximately 500-ms steps to 20 mV from a holding potential of −60 mV. *C*: graph showing amplitude histogram obtained from unitary currents at 20-mV step potential. *D*: single-channel *I–V* relations obtained from control patches (○, $n = 6$) and NO-modified patches (●, $n = 6$) (100 nM NO solution was superfused in the bath). The calculated conductances were 275 ± 11 pS ($n = 6$) and 280 ± 17 pS ($n = 6$, $P = 0.6$) for control and NO-modified patches, respectively. *E*: diary plot of the open probability of a cell-attached Ca^{2+}-activated K^+ current (BK) channel patch as a complement of time, showing the drastic increase in P_o in the presence of NO vs. control and the reversal effects of DTT (0.2 mM).

et al. 2002). However, what is most unclear is the physiological significance of NO release.

The efferent nerve system, projecting to the inner ear or its homologue, from the olivocochlear pathway exists in a wide range of organisms, raising the possibility that evolutionary preservation of the system is of vital importance to inner ear functions (Dilly 1976; Guinan Jr et al. 1983). For example, ACh is the neurotransmitter released by the medial efferent fibers and analogous synaptic feedback has been identified in hair cells of the fish lateral line, amphibian, and avian inner ear (Eybalin 1993). ACh released from efferent nerve terminals produces fast hyperpolarization of hair cells by activating Ca^{2+}-dependent small conductance (SK) K^+ channels (Elgoyhen et al. 2001; Housley et al. 2006). Moreover, repetitive shock trains of efferent fibers produce a second slow hyperpolarization, but the underlying mechanism remains unaccountable (Sridhar et al. 1997). The unique expression and tissue specificity in efferent terminals and hair cells (Fessenden and Schacht 1998; Lysakowski and Singer 2000) indicate that NOS might serve specialized physiological functions. Indeed, it has been suggested that NO release either from hair cells or efferent nerve terminals might mediate negative feedback mechanisms on hair cells (Fessenden and Schacht 1998). Moreover, the effects of NO on hair cells cannot be generalized since it appears to have opposing actions on other hair-cell types (Chen and Eatock 2000). NO-mediated activation of cyclic nucleotides and its relevance efferent system modulation of hair cells and cochlear amplification dovetail well with previous studies (Dek et al. 2005; Szönyi et al. 1999). Overall, the present findings contribute to the growing awareness that actions of NO in the operational status of hair cells may provide an essential mechanism for custom modulation of hair-cell functions.

GRANTS

This work was supported by a Deafness Research Foundation grant to P. Yevgeniy, a National Center for Research Resources Grant P41-RR-01395 to P.J.S. Smith, and National Institute on Deafness and Other Communication Disorders Grants DC-003826 and DC-007592 to E. N. Yamoah.

DISCLOSURES

No conflicts of interest are declared by the authors.

REFERENCES

Ahmmed GU, Xu Y, Hong Dong P, Zhang Z, Eiserich J, Chiamvimonvat N. Nitric oxide modulates cardiac Na(+) channel via protein kinase A and protein kinase G. *Circ Res* 89: 1005–1013, 2001.

Almanza A, Navarrete F, Vega R, Soto E. Modulation of voltage-gated Ca^{2+} current in vestibular hair cells by nitric oxide. *J Neurophysiol* 97: 1188–1195, 2007.

Armstrong CE, Roberts WM. Electrical properties of frog saccular hair cells: distortion by enzymatic dissociation. *J Neurosci* 18: 2962–2973, 1998.

Armstrong CE, Roberts WM. Rapidly inactivating and non-inactivating calcium-activated potassium currents in frog saccular hair cells. *J Physiol* 536: 49–65, 2001.

Art JJ, Fettiplace R, Wu YC. The effects of low calcium on voltage-dependent conductances involved in tuning of turtle hair cells. *J Physiol* 470: 109–126, 1993.

Art JJ, Wu YC, Fettiplace R. The calcium-activated potassium channels of turtle hair cells. *J Gen Physiol* 105: 49–72, 1995.

Bredt DS, Hwang PM, Snyder SH. Localization of nitric oxide synthase indicating a neural role for nitric oxide. *Nature* 347: 768–770, 1990.

Campbell DL, Stamler JS, Strauss HC. Redox modulation of L-type calcium channels in ferret ventricular myocytes. Dual mechanism regulation by nitric oxide and S-nitrosothiols. *J Gen Physiol* 108: 277–293, 1996.

Chabbert CH. Heterogeneity of hair cells in the bullfrog sacculus. *Pflügers Arch* 435: 82–90, 1997.

Chen C, Nenov A, Skellett R, Fallon M, Bright L, Norris CH, Bobbin RP. Nitroprusside suppresses cochlear potentials and outer hair cell responses. *Hear Res* 87: 1–8, 1995.

Chen JW, Eatock RA. Major potassium conductance in type I hair cells from rat semicircular canals: characterization and modulation by nitric oxide. *J Neurophysiol* 84: 139–151, 2000.

Chvanov M, Gerasimenko OV, Petersen OH, Tepikin AV. Calcium-dependent release of NO from intracellular S-nitrosothiols. *EMBO J* 25: 3024–3032, 2006.

Colquhoun D, Sigworth FJ. Editors. *Fitting and Statistical Analysis of Single-Channel Records*. New York: Plenum, 1985.

Crawford AC, Fettiplace R. An electrical tuning mechanism in turtle cochlear hair cells. *J Physiol* 312: 377–412, 1981.

Dek L, Zheng J, Orem A, Du GG, Aguiaga S, Matsuda K, Dallos P. Effects of cyclic nucleotides on the function of prestin. *J Physiol* 563: 483–496, 2005.

Dilly PN. The structure of some cephalopod statoliths. *Cell Tissue Res* 175: 147–163, 1976.

Elgoyhen AB, Vetter DE, Katz E, Rothlin CV, Heinemann SF, Boulter J. alpha10: a determinant of nicotinic cholinergic receptor function in mammalian vestibular and cochlear mechanosensory hair cells. *Proc Natl Acad Sci USA* 98: 3501–3506, 2001.

Eybalin M. Neurotransmitters and neuromodulators of the mammalian cochlea. *Physiol Rev* 73: 309–373, 1993.

Fessenden JD, Coling DE, Schacht J. Detection and characterization of nitric oxide synthase in the mammalian cochlea. *Brain Res* 668: 9–15, 1994.

Fessenden JD, Schacht J. The nitric oxide/cyclic GMP pathway: a potential major regulator of cochlear physiology. *Hear Res* 118: 168–176, 1998.

Flores A, Soto E, Vega R. Nitric oxide in the afferent synaptic transmission of the axolotl vestibular system. *Neuroscience* 103: 457–464, 2001.

Friedemann MN, Robinson SW, Gerhardt GA. o-Phenylenediamine-modified carbon fiber electrodes for the detection of nitric oxide. *Anal Chem* 68: 2621–2628, 1996.

Fuchs PA. Ionic currents in cochlear hair cells. *Prog Neurobiol* 39: 493–505, 1992.

Fuchs PA, Evans MG. Voltage oscillations and ionic conductances in hair cells isolated from the alligator cochlea. *J Comp Physiol A Sens Neural Behav Physiol* 164: 151–163, 1988.

Gosepath K, Gath I, Maurer J, Pollock JS, Amedee R, Forstermann U, Mann W. Characterization of nitric oxide synthase isoforms expressed in different structures of the guinea pig cochlea. *Brain Res* 747: 26–33, 1997.

Guinan JJ Jr, Warr WB, Norris BE. Differential olivocochlear projections from lateral versus medial zones of the superior olivary complex. *J Comp Neurol* 221: 358–370, 1983.

Hamill OP, Marty A, Neher E, Sakmann B, Sigworth FJ. Improved patch-clamp techniques for high-resolution current recording from cells and cell-free membrane patches. *Pflügers Arch* 391: 85–100, 1981.

Han X, Kobzik L, Severson D, Shimoni Y. Characteristics of nitric oxide-mediated cholinergic modulation of calcium current in rabbit sino-atrial node. *J Physiol* 509: 741–754, 1998.

Hess A, Bloch W, Arnhold S, Andressen C, Stennert E, Addicks K, Michel O. Nitric oxide synthase in the vestibulocochlear system of mice. *Brain Res* 813: 97–102, 1998.

Holt JR, Corey DP, Eatock RA. Mechanoelectrical transduction and adaptation in hair cells of the mouse utricle, a low-frequency vestibular organ. *J Neurosci* 17: 8739–8748, 1997.

Housley GD, Marcotti W, Navaratnam D, Yamoah EN. Hair cells: beyond the transducer. *J Membr Biol* 209: 89–118, 2006.

Hudspeth AJ, Lewis RS. Kinetic analysis of voltage- and ion-dependent conductances in saccular hair cells of the bull-frog, *Rana catesbeiana*. *J Physiol* 400: 237–274, 1988a.

Hudspeth AJ, Lewis RS. A model for electrical resonance and frequency tuning in saccular hair cells of the bull-frog, *Rana catesbeiana*. *J Physiol* 400: 275–297, 1988b.

Hudspeth AJ, Logothetis NK. Sensory systems. *Curr Opin Neurobiol* 10: 631–641, 2000.

Jiang ZG, Shi X, Zhao H, Si JQ, Nuttall AL. Basal nitric oxide production contributes to membrane potential and vasotone regulation of guinea pig in vitro spiral modiolar artery. *Hear Res* 189: 92–100, 2004.

Katz E, Elgoyhen AB, Gomez-Casati ME, Knipper M, Vetter DE, Fuchs PA, Glowatzki E. Developmental regulation of nicotinic synapses on cochlear inner hair cells. *J Neurosci* 24: 7814–7820, 2004.

Korn SJ, Marty A, Connor JA, Horn R. Perforated patch recording. *Methods Neurosci* 4: 264–373, 1991.

Kumar SM, Porterfield DM, Muller KJ, Smith PJ, Sahley CL. Nerve injury induces a rapid efflux of nitric oxide (NO) detected with a novel NO microsensor. *J Neurosci* 21: 215–220, 2001.

Land SC, Porterfield DM, Sanger RH, Smith PJ. The self-referencing oxygen-selective microelectrode: detection of transmembrane oxygen flux from single cells. *J Exp Biol* 202: 211–218, 1999.

Lysakowski A, Singer M. Nitric oxide synthase localized in a subpopulation of vestibular efferents with NADPH diaphorase histochemistry and nitric oxide synthase immunohistochemistry. *J Comp Neurol* 427: 508–521, 2000.

Michel O, Hess A, Bloch W, Stennert E, Su J, Addicks K. Localization of the NO/cGMP-pathway in the cochlea of guinea pigs. *Hear Res* 133: 1–9, 1999.

Mistry DK, Garland CJ. Nitric oxide (NO)-induced activation of large conductance Ca^{2+}-dependent K^+ channels (BK(Ca)) in smooth muscle cells isolated from the rat mesenteric artery. *Br J Pharmacol* 124: 1131–1140, 1998.

Porterfield DM, Laskin JD, Jung SK, Malchow RP, Billack B, Smith PJ, Heck DE. Proteins and lipids define the diffusional field of nitric oxide. *Am J Physiol Lung Cell Mol Physiol* 281: L904–L912, 2001.

Riemann R, Reuss S. Nitric oxide synthase in identified olivocochlear projection neurons in rat and guinea pig. *Hear Res* 135: 181–189, 1999.

Roberts WM, Jacobs RA, Hudspeth AJ. Colocalization of ion channels involved in frequency selectivity and synaptic transmission at presynaptic active zones of hair cells. *J Neurosci* 10: 3664–3684, 1990.

Rodriguez-Contreras A, Nonner W, Yamoah EN. Ca^{2+} transport properties and determinants of anomalous mole fraction effects of single voltage-gated Ca^{2+} channels in hair cells from bullfrog saccule. *J Physiol* 538: 729–745, 2002.

Rodriguez-Contreras A, Yamoah EN. Direct measurement of single-channel Ca(2+) currents in bullfrog hair cells reveals two distinct channel subtypes. *J Physiol* 534: 669–689, 2001.

Rodriguez-Contreras A, Yamoah EN. Effects of permeant ion concentrations on the gating of L-type Ca^{2+} channels in hair cells. *Biophys J* 84: 3457–3469, 2003.

Ruppersberg JP, Stocker M, Pongs O, Heinemann SH, Frank R, Koenen M. Regulation of fast inactivation of cloned mammalian IK(A) channels by cysteine oxidation. *Nature* 352: 711–714, 1991.

Shafer OT, Chen A, Kumar SM, Muller KJ, Sahley CL. Injury-induced expression of endothelial nitric oxide synthase by glial and microglial cells in the leech central nervous system within minutes after injury. *Proc Biol Sci* 265: 2171–2175, 1998.

Shi X, Ren T, Nuttall AL. The electrochemical and fluorescence detection of nitric oxide in the cochlea and its increase following loud sound. *Hear Res* 164: 49–58, 2002.

Singer M, Lysakowski A. Nitric oxide synthase localized in a subpopulation of vestibular efferents with NADPH diaphorase histochemistry. *Ann NY Acad Sci* 781: 658–662, 1996.

Smith PJ, Hammar K, Porterfield DM, Sanger RH, Trimarchi JR. Self-referencing, non-invasive, ion selective electrode for single cell detection of trans-plasma membrane calcium flux. *Microsc Res Tech* 46: 398–417, 1999.

Snyder SH. Nitric oxide and neurons. *Curr Opin Neurobiol* 2: 323–327, 1992.

Snyder SH, Bredt DS. Biological roles of nitric oxide. *Sci Am* 266: 68–71, 74–67, 1992.

Song T, Hatano N, Kambe T, Miyamoto Y, Ihara H, Yamamoto H, Sugimoto K, Kume K, Yamaguchi F, Tokuda M, Watanabe Y. Nitric oxide-mediated modulation of calcium/calmodulin-dependent protein kinase II. *Biochem J* 412: 223–231, 2008.

Sridhar TS, Brown MC, Sewell WF. Unique postsynaptic signaling at the hair cell efferent synapse permits calcium to evoke changes on two time scales. *J Neurosci* 17: 428–437, 1997.

Stamler JS, Loscalzo J. Endothelium-derived relaxing factor modulates the atherothrombogenic effects of homocysteine. *J Cardiovasc Pharmacol* 20, Suppl. 12: S202–S204, 1992.

Stamler JS, Singel DJ, Loscalzo J. Biochemistry of nitric oxide and its redox-activated forms. *Science* 258: 1898–1902, 1992.

Szönyi M, He DZZ, Ribári O, Sziklai I, Dallos P. Cyclic-GMP and outer hair cell electromotility. *Hear Res* 137: 29–42, 1999.

Vega R, Ortega A, Almanza A, Soto E. Nitric oxide in the amphibian (*Ambystoma tigrinum*) lateral line. *Neurosci Lett* 393: 65–69, 2006.

Yoshida N, Hequembourg SJ, Atencio CA, Rosowski JJ, Liberman MC. Acoustic injury in mice: 129/SvEv is exceptionally resistant to noise-induced hearing loss. *Hear Res* 141: 97–106, 2000.

Yuhas WA, Fuchs PA. Apamin-sensitive, small-conductance, calcium-activated potassium channels mediate cholinergic inhibition of chick auditory hair cells. *J Comp Physiol A Sens Neural Behav Physiol* 185: 455–462, 1999.